

Effect of Local Topological Changes on Resistance in Tunably-Disordered Networks

Chenxi Wang, Charles Emmett Maher, and Katherine A. Newhall*

Department of Mathematics, University of North Carolina at Chapel Hill, Chapel Hill, NC, USA

(Dated: February 5, 2026)

Disordered materials occur naturally and also provide a broader design space than ordered or crystalline structures. We investigate a two-dimensional disordered network metamaterial constructed from a Delaunay triangulation of an underlying point cloud. Small perturbations in the point cloud induce discrete topological changes. One such change we identify is a Delaunay flip, in which two neighboring Delaunay triangles that form a convex quadrilateral structure with their common edge being one of the two quadrilateral diagonals exchange this diagonal for the other diagonal. These topological changes can cause substantial jumps in the effective resistance measured diagonally across the network, when the change is located near the source or the sink node. The jumps are explained analytically by showing that the change in effective resistance from edge removal or addition depends on the voltage drop across that edge. However, Delaunay flips have less impact on global resistance measurements and in larger networks. These local topological changes are relevant for finite-sized samples and experimentally-measurable properties such as electrical transport. Global characterizations of the network disorder or topology lack the location-specificity of our observed effects on network transport, and thus may be inadequate for predicting certain experimentally measurable transport properties in disordered network metamaterials, highlighting the importance of localized regions in material design.

I. INTRODUCTION

Disordered networks are used to model the behaviors of systems across the physical sciences including polymers [1], metallic foams [2], two-dimensional (2D) materials [3, 4], actin networks [5], slime molds [6], and power grids [7] among several others (see, e.g., Ref. [8] and references therein for additional examples). Disorder in network systems has been shown to impart desirable properties including resistance to fracture [9], exotic vibrational properties [10], and extraordinary elastic properties [11–13]. Due to the large design space available to disordered network structures, and their notable physical properties, a number of recent works have focused on characterizing the structure [14–16] and properties [17–19] of disordered network metamaterials as well as methods to manufacture them [20].

Of specific interest are the electrical transport properties of network structures. Such properties have been studied, e.g., through the lens of effective properties for two-phase materials [11, 13] as well as density functional theory [21]. Here, we focus on a network science approach, which treats the edges in the network as either wires or lumped circuit elements (in the metric network case) or resistors (in the combinatorial network case). The metric network framework has been used to model how signals travel through systems like transmission lines and electrical networks [22–31]. Numerous studies have focused on the resistance of combinatorial networks in a mathematical setting (see, e.g., Refs. [8, 32–37]), but fewer studies have used a network framework to explicitly model the electrical transport in materials, e.g., Refs. [4, 38].

In Ref. [4], Obrero *et al.* computed the effective resistance of a series of finite-sized disordered networks generated by computing the Delaunay triangulation of a totally uncorrelated point cloud evolved via repeated applications of Lloyd’s algorithm [39] (see Sec. II A for details). There, the authors noted sharp changes (“jumps”) in the effective resistance that do not correlate with the degree of short or long-range translational disorder in the network. Standard methods of characterizing network structures that typically indicate sharp changes in network properties, such as those indicating the onset of failure processes in materials [40], were not found to capture the observed jumps in resistance. Thus, the authors suggested that topological changes in the network result in these jumps, which is supported by network topological changes affecting the physical and mathematical properties of networks including, e.g., electrical transport [21, 41], wave transport [42], fracture mechanisms [43, 44], and spectral properties [36, 45, 46].

Inspired by these observations from Ref. [4], we aim to characterize the effect of the topology of a network on its electric transport properties. Specifically, we characterize the topological changes that occur in the finite-sized networks studied in Ref. [4] and how they affect the measurement of the effective resistance. We demonstrate that the construction of the Delaunay triangulation from a set of points evolved using Lloyd’s algorithm results in discontinuous changes in network topology that include the addition of edges along the boundary of a finite-sized network and concerted deletion and addition of single edges (which we call “Delaunay flips”). We show that topological changes that occur near the nodes between which the effective resistance R_{eff} is measured coincide with the large jumps in R_{eff} observed in Ref. [4], while changes further away from those nodes have a much smaller impact on R_{eff} . We support these numerical results with an an-

* Contact author: knewhall@unc.edu

alytical approximation based on the Sherman–Morrison formula [47]. We contrast these Delaunay triangulation results with the corresponding Voronoi tessellations of the same point cloud evolving under Lloyd’s algorithm, whose structural changes result in a much smoother evolution of R_{eff} as the point cloud evolves. Moreover, we show that the total effective resistance R_{tot} , which is a global quantification of the electrical transport properties of a network, is much less sensitive to local topological changes than R_{eff} , and does not effectively capture the effect of topology on the experimentally relevant R_{eff} measurement. These findings suggest that global structural descriptors may obfuscate the structural characteristics that are important to certain physical properties, especially those that are relevant to the characterization of the physical properties of finite systems in experimental contexts.

The rest of this paper is organized as follows. In Sec. II, we describe the construction of the networks analyzed in this work, how we characterize their effective resistances, and the methods used to study the effect of network topology on effective resistance. Then, in Sec. III, we characterize the effect of network topology on effective resistance via computation and present a method to analytically approximate the change in effective resistance due to topological changes. Finally, in Sec. IV, we discuss our findings and offer conclusions and outlook for future studies.

II. METHODS

A. Network Generation

We study the disordered network metamaterials created in Ref. [4]. These quasi-2D materials have relatively smooth and systematic evolution toward order, measured by the edge or node entropy. To generate such a sequence of networks, an initial totally uncorrelated point cloud of N points is evolved within a bounding box with Lloyd’s algorithm [39], which has been shown to progress logarithmically towards a crystalline configuration [48, 49]. This algorithm repeatedly computes the Voronoi tessellation [8] within the bounding box and moves each point to the centroid of its Voronoi cell. After L iterations of the algorithm, the points are connected with a Delaunay triangulation [8] to form a connected network. To generate the Delaunay triangulation, sets of 3 points in the point cloud are connected in a triangle if the circumcircle of those three points does not contain any other points in the pattern. This geometric constraint is the *Delaunay criterion*. We also consider the Voronoi tessellation of these point clouds, which involves finding the polygonal regions of space (Voronoi cells) closer to one point than to any other point in the progenitor point cloud. Note that one can also generate the Delaunay triangulation by adding an edge between points whose Voronoi cells share an edge. We then treat the edges and nodes of the poly-

gons from these two tessellation schemes as the edges and nodes of our networks.

B. Electrical Transport

To understand a network’s electrical transport properties, we treat the network edges as ohmic resistors that connect at the nodes. Obrero *et al.* [4] derived a mathematical model of the effective resistance diagonally across the network and validated resistance values computed using this model against experimental measurements of the physical samples 3D printed out of Ti-64-4V. Next, we summarize this derivation based on applying Kirchhoff’s conservation of current law at each node and Kirchhoff’s voltage law along each edge to calculate both the effective resistance between any two nodes in the network and the total effective resistance, defined as the sum of the effective resistance over all pairs of nodes. This derivation closely follows the one found in Ref. [50] and is written in terms of the weighted combinatorial graph Laplacian, an adaptation of the more common $\mathcal{L}_U \vec{V} = r \vec{I}$ in the literature (for example, see Refs. [51, 52]) that uses an unweighted graph Laplacian \mathcal{L}_U and a constant resistance r for all edges.

The resistance of the edge connecting node i to node j is

$$R_{ij} = \frac{a}{\rho \ell_{ij}} \quad \text{for } i, j = 1 \dots N, i \neq j,$$

where ρ is the resistivity of Ti-64-4V ($178 \mu\Omega \text{ cm}$), a is the fixed cross-sectional area of each edge ($a = 0.03 \text{ cm}^2$) and ℓ_{ij} is the length of each edge. These specific parameter choices correspond to the 3D printed networks from Ref. [4]. By defining the weighted adjacency matrix as

$$A_{ij} = \begin{cases} \frac{1}{R_{ij}} & \text{if } i \text{ and } j \text{ are connected,} \\ 0 & \text{otherwise.} \end{cases}$$

Kirchhoff’s laws lead to the equations

$$\sum_{j=1}^N A_{ij} (V_i - V_j) = I_i \quad \text{for } i = 1 \dots N,$$

where V_i and V_j are the voltage at nodes i and j respectively, and I_i is the current injected into node i . Defining the weighted degree matrix D with diagonal elements equal to the sum of the weights of the edges connected at node i , $D_{ii} = \sum_{j=1}^N A_{ij}$ and the weighted graph Laplacian matrix $\mathcal{L} = D - A$, the above in matrix form is

$$\mathcal{L} \vec{V} = \vec{I}, \tag{1}$$

where \vec{V} and \vec{I} are the vectors of the voltages and injected currents at each node i . Note that for a network with only one connected component the Laplacian matrix is rank $N - 1$ [52], consistent with the fact that only the voltage

difference can be uniquely determined; in practice, we set the sink node voltage to zero and solve for the remaining $N - 1$ voltages.

To compute the effective resistance between any two nodes i and j , we inject $I_0 = 10$ mA of current into node i , and remove the same amount from node j , so that the current injection vector \vec{I} is

$$I_k = \begin{cases} I_0 & \text{if } k = i, \\ -I_0 & \text{if } k = j, \\ 0 & \text{otherwise.} \end{cases} \quad (2)$$

By solving the linear system for \vec{V} , we obtain the effective resistance between any two nodes i and node j as

$$R_{\text{eff}}^{ij} = \frac{|V_i - V_j|}{I_0}.$$

Here, we are specifically interested in the experimental configuration A from Ref. [4], thus we refer to R_{eff} as the effective resistance diagonally across the network from the northeast-most node to the southwest-most node. One example of this configuration, and the resulting voltage at each node, is shown in Fig. 1A.

We also calculate the total effective resistance, also called the Kirchhoff's index, that quantifies the network's global electrical properties. It is the pairwise sum of all the effective resistances,

$$R_{\text{tot}} = \sum_{1 \leq i < j \leq N} R_{\text{eff}}^{ij},$$

which is equivalent to N times the sum of the inverse of the non-zero eigenvalues λ_k of the weighted graph Laplacian matrix [53, 54],

$$R_{\text{tot}} = N \text{ Tr}(\mathcal{L}^+) = N \sum_{k=2}^N \frac{1}{\lambda_k}, \quad (3)$$

where \mathcal{L}^+ is the Moore-Penrose pseudoinverse [55] of the weighted graph Laplacian matrix.

C. Edge Flip Enumeration Algorithm

Here we describe the *edge flip enumeration test*, which we designed to show the spatially heterogeneous response of single topological changes on either R_{eff} or R_{tot} . Algorithm 1 first enumerates all network edges that are part of two neighboring triangles that form a convex quadrilateral with their common edge being one of the two quadrilateral diagonals. Next, each enumerated diagonal edge is independently flipped to the alternate diagonal, and the resulting resistance changes are recorded. This topological change is similar to the Delaunay flip we observe between successive iterations of Lloyd's algorithm; however, the edge flip enumeration test can be performed

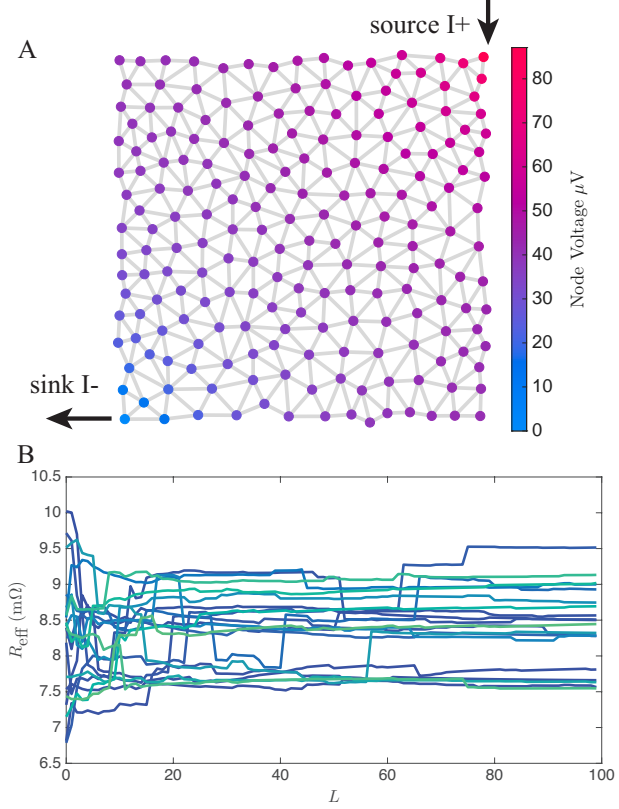


Figure 1. A: Schematic showing the source and sink nodes used to compute R_{eff} diagonally across the network. Nodes are colored by their voltage, computed with Eq. (1). B: Effective resistance R_{eff} as a function of Lloyd's iteration number, showing jumps between successive Lloyd's iterations. Each curve follows the evolution of a different initial point cloud.

on any network with the aforementioned convex quadrilateral structures. More generally, one could probe the effect of removing any edge in the network and adding another edge as long as the added edge does not cross an existing edge, thus keeping the network spatially embedded. Note that since we manually impose the diagonal flip, if applied to a Delaunay triangulation, the resulting network is now in violation of the Delaunay criterion.

D. Tortuosity

Tortuosity is the ratio of the shortest-path distance between two nodes in a spatially embedded network and the Euclidean distance between the two nodes. Therefore, a tortuosity value of one indicates a perfectly straight path between two network nodes, while a larger value corresponds to a more indirect path. We calculate the change in tortuosity across a convex quadrilateral structure in a network when the edge flip test is applied to that quadrilateral as a way to help explain the magnitude of effective resistance change. Specifically, we identify quadrilaterals whose

Algorithm 1: Edge Flip Enumeration Test

Input: A , the weighted adjacency matrix of the network
Output: ΔR_{eff} , ΔR_{tot} resistance change for each diagonal edge flip

```

1: Compute original  $R_{\text{eff}}$ ,  $R_{\text{tot}}$ 
2: Enumerate all triangles in the network
3: Enumerate all edges connecting nodes  $i$  and  $j$  with
   ( $i < j$ )
4: Form a mapping between each edge and the triangles
   the edge belongs to.
5: for each edge  $e_{ij}$  do
6:   if  $e_{ij}$  belongs to at least two triangles then
7:     Check convexity of the quadrilateral
8:     if convex then
9:       Delete edge  $e_{ij}$ 
10:      Add edge of opposite diagonal in quadrilateral
11:      Compute new  $R_{\text{eff}}$ ,  $R_{\text{tot}}$ ; calculate
     $\Delta R_{\text{eff}}$ ,  $\Delta R_{\text{tot}}$ 
12:      Return network to its original state
13:    end if
14:  end if
15: end for

```

sets of nodes contain either the source or sink node for a network. Then, we label the quadrilateral nodes $a-c-b-d$ with node a the source or sink node, depending on the location in the network of the identified quadrilateral. If there is an edge connecting node a to node b , the tortuosity is equal to one, as the network path is the same as the Euclidean length. If there is not an edge, then the tortuosity is

$$\tau_{ab} = \frac{C_{ab}}{l_{ab}},$$

where l_{ab} is the Euclidean distance between nodes a and b and the path length along the quadrilateral edges is

$$C_{ab} = \min(l_{ac} + l_{bc}, l_{ad} + l_{bd}).$$

Thus, the change in tortuosity when the edge flip test is applied to the quadrilateral is

$$\Delta\tau_{ab} = |1 - \tau_{ab}|. \quad (4)$$

III. RESULTS

A. Jumps in Effective Resistance are caused by local topological changes near source/sink nodes

Using Lloyd's algorithm and the Delaunay triangulation to create a sequence of networks that begin disordered and progress towards ordered, Obrero *et al.* [4]

observed large jumps in the effective resistance between sequential Lloyd's iterations. These jumps can be seen in Fig. 1B, where effective resistance, R_{eff} , for an $N = 200$ node network is plotted vs. Lloyd's iteration number, L , and each curve corresponds to a different initial point cloud. While these jumps are accompanied by a topological change in the adjacency matrix (adding or removing edges), not all topological changes in the adjacency matrix corresponded to a large jump in R_{eff} . Here, we explain these jumps, finding that edges near the northeast and southwest corners of the network, where current is applied, have a larger impact on R_{eff} .

In Fig. 2, we show examples of the two topological changes responsible for the large jumps. Fig. 2A highlights just one initial point cloud (simulation 14 from Ref. [4]) and two jumps in R_{eff} , one from $L = 14$ to $L = 15$ and one from $L = 57$ to $L = 58$. The networks before and after the first (second) jump are depicted in Figs. 2B and C (D and E). The jump labeled B→C coincides with the addition of an edge along the boundary

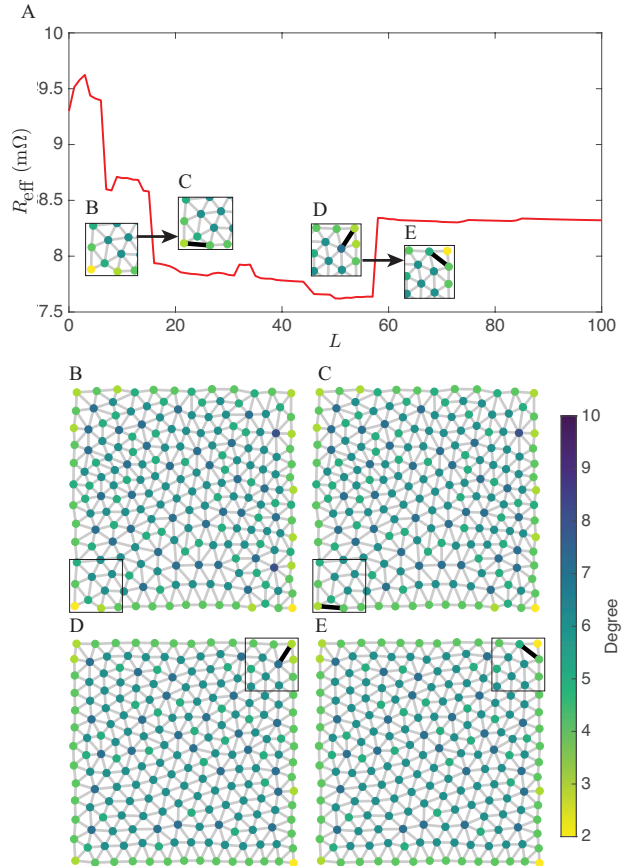


Figure 2. A: The progression of R_{eff} under Lloyd's iterations for one simulation, highlighting two jumps and two topological changes. The insets B and C highlight in black the addition of an edge at the bottom left corner of the network; the full networks are shown in panels B and C. The insets D and E highlight in black the Delaunay flip in the top right corner of the network; the full networks are shown in panels D and E.

at the southwest corner. The new edge is marked with a thick black line in Fig. 2C. The jump labeled D→E coincides with the flip of one edge inside the quadrilateral structure at the northeast corner. This flipped edge is marked with thick black lines in Figs. 2D and E.

As all of the nodes move between successive Lloyd's iterations, we also check how the above-identified topological changes affect R_{eff} in isolation. Keeping the network fixed in the configuration before the jump, we manually perform the single topological change (adding a single edge or flipping a single edge) and recompute R_{eff} . These values of R_{eff} are summarized in Table I for a number of example jumps. We compute how much of the true jump this single topological change accounts for by dividing the true jump in R_{eff} by the manual jump. In all cases, nearly 100% of the jump is accounted for with this single topological change. (Accounting for over 100% simply indicates the topological change in isolation results in a larger jump than observed.) These results provide strong evidence that a single topological change is sufficient to explain the observed jump in effective resistance.

The two topological changes (Delaunay flip and edge addition) occur abruptly even though the underlying points of the Delaunay triangulation undergo small changes, especially at higher values of L . Figure 3 depicts the two mechanisms: panels A, B and C depict the edge flip, a result of the Delaunay criterion as points get perturbed, and panels D and E depict the edge addition, primarily driven by the imposed boundary. Figure 3A depicts two circumcircles for four points in the form of a quadrilateral with one diagonal. Figure 3B shows the same circumcircles but now with the points perturbed

| R_{eff} Jump | Type | Before | After | Manual | Accounted |
|--------------------------|------|--------|--------|--------|-----------|
| sim3 iter3-4 | Add | 9.7011 | 8.7956 | 8.8533 | 93.6% |
| sim4 iter6-7 | Flip | 8.6439 | 7.8119 | 7.8641 | 93.7% |
| sim6 iter9-10 | Flip | 7.6916 | 8.3276 | 8.3347 | 101.1% |
| sim6 iter12-13 | Flip | 8.3214 | 8.974 | 8.9648 | 98.6% |
| sim6 iter52-53 | Add | 9.0918 | 8.5121 | 8.5127 | 99.9% |
| sim7 iter4-5 | Add | 8.5839 | 7.8772 | 7.8814 | 99.4% |
| sim7 iter20-21 | Flip | 7.7698 | 8.5498 | 8.543 | 99.1% |
| sim8 iter23-24 | Flip | 7.9019 | 8.6116 | 8.5755 | 94.9% |
| sim10 iter28-29 | Flip | 8.5531 | 7.9436 | 7.9582 | 97.6% |
| sim10 iter41-42 | Flip | 7.8338 | 8.5768 | 8.5827 | 100.8% |
| sim10 iter66-67 | Flip | 8.5041 | 9.1118 | 9.1104 | 99.8% |
| sim14 iter6-7 | Add | 9.3958 | 8.5991 | 8.5937 | 100.7% |
| sim14 iter14-15 | Add | 8.5796 | 7.9373 | 7.9275 | 101.5% |
| sim14 iter57-58 | Flip | 7.6367 | 8.3427 | 8.3447 | 100.3% |

Table I. Values of R_{eff} before and after a topological change in the networks from Ref. [4]. “Type” indicates whether this topological change was the addition of an edge (“Add”) or a Delaunay flip (“Flip”). The columns “Before” and “After” contain the true value of R_{eff} before and after the jump, respectively. The column “Manual” contains the value after the single topological change identified in column “Type” is executed manually. The column “Accounted” is calculated as $(\text{Manual} - \text{Before}) / (\text{After} - \text{Before})$.

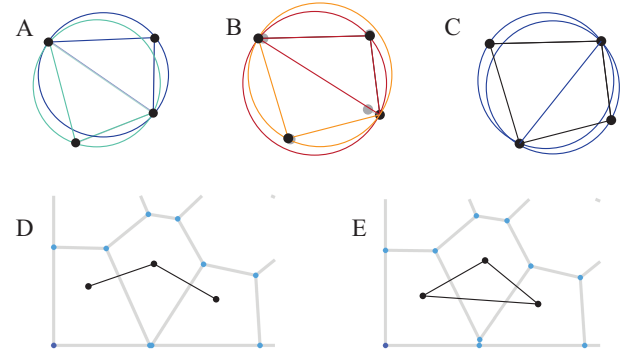


Figure 3. Mechanisms of topological changes. Delaunay flip occurs between panel A and C, with panel B illustrating how the Delaunay criterion is violated as a result of one node moving from the gray location. An edge addition at the boundary occurs between panels D and E, where the Voronoi tessellation is shown with blue nodes and gray edges and the Delaunay triangulation for these three complete cells is shown in black.

from their original gray position to their new black position. The dark blue (light blue) circle evolves to the dark red (light orange) circle and now contains the lower-left (upper-right) point within it; the Delaunay criterion is not met. Flipping the diagonal, shown in Fig. 3C, yields an edge configuration satisfying the Delaunay criterion. The edge addition is a result of computing the Voronoi tessellation in a bounded, rather than infinite, domain. Recall connecting points of bordering Voronoi cells is an alternative method from the Delaunay criterion for constructing the Delaunay triangulation. Figure 3D shows part of the Delaunay triangulation in black for the three Voronoi cells at the boundary of the domain. After the points are perturbed under one iteration of Lloyd's algorithm, the center Voronoi cell no longer intersects the boundary, allowing the two other Voronoi cells to share a boundary. This results in the addition of a third Delaunay edge, as shown in Fig. 3E.

Having numerically verified that a single edge flip can account for nearly the entire jump in R_{eff} , we further hypothesize that only changes local to the source or sink node cause these large jumps in resistance. To numerically support this hypothesis, we start with a simpler case: a 15×15 square lattice with the southwest to northeast diagonal of each unit connected, as depicted in Fig. 4A. We independently flip each interior edge while keeping the others unflipped, reporting the magnitude of the percentage change in R_{eff} in the heat map shown in Fig. 4B. We observe that edges along the northeast-southwest diagonal have the largest effect on R_{eff} , with the most significant change being from the edges directly in contact with the source or the sink node.

To further test this sensitivity to topological perturbation near the source or sink node, we perform a similar flip-test on the random networks generated by the method of Sec. II A. First, we identify all convex quadri-

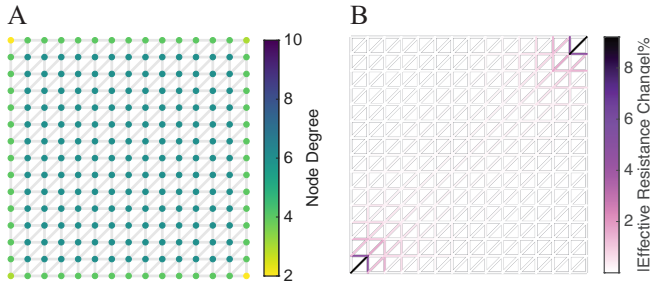


Figure 4. A: Simplified lattice network. B: Heatmap where the color of each edge indicates the magnitude of the relative percent change of the effective resistance, R_{eff} , when the edge is flipped to the other diagonal of its quadrilateral. Boundary edges are not flipped, and are colored white (i.e. zero change).

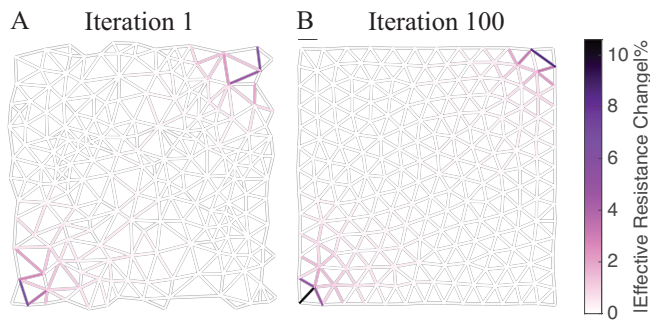


Figure 5. Heatmap where the color of each edge indicates the magnitude of the relative percent change of the effective resistance, R_{eff} , when the edge is flipped to the other diagonal of its quadrilateral. Boundary edges and those not part of a convex quadrilateral are not flipped, and are colored white (i.e. zero change).

lateral in the network as explained in Sec. II C. Then, as with the simple lattice network, we independently flip the diagonal in each quadrilateral while keeping the others unflipped, reporting the absolute value of the percent change in R_{eff} in Fig. 5. Consistent with the lattice network, edges near the source and sink nodes have the greatest effect. Note that in the lattice network, flipping the diagonal of each square cell always resulted in an increase in R_{eff} since each edge was being flipped from parallel to perpendicular to the diagonal of the current application. In the random networks, we see both increase and decrease depending on edge-orientation; we only present the magnitude of the change. This is because in the lattice network, the cell diagonals are all aligned in the direction from the source to the sink node. Flipping any one diagonal disrupts this and thus increases the effective resistance. In the disordered networks, the diagonals are not all aligned in the same direction, thus a flip may help or hinder the flow of current from source to sink node.

B. Predicting Location of Topological Change Producing Largest Effective Resistance Jumps

In Sec. III A, we identified that edges near the source and sink nodes have the greatest effect on the effective resistance. Here, we further explore this finding over an ensemble of networks, revealing that closeness to source/sink nodes alone is not enough to predict the magnitude of the effect of a topological change on the effective resistance. We analytically approximate the effect of a Delaunay flip on the effective resistance, finding that it depends on the voltage difference across the flipped edge, thereby supporting that the location of edges responsible for the largest changes in R_{eff} are located near the source and sink nodes where voltage differences are highest, but also that longer edges produce larger differences in effective resistance.

In Fig. 6A, we plot the location of the center of the edge responsible for the maximal magnitude of change in R_{eff} when performing the edge flip test. This was performed on 20 simulations at each iteration of Lloyd's algorithm, $L = 0$ to $L = 100$. All edges responsible for maximal change are in the vicinity of the source or sink node. By further investigating individual networks with some of the largest maximum effective resistance changes, we notice that edge length also plays a role in the magnitude of the change in effective resistance. Specifically, networks with high maximum percentage change seem to have highly oblique quadrilaterals with one short and one large diagonal. One such example appears in the lower-left corner of the network in Fig. 6D. To further understand and predict these network features that affect drastic changes on the effective resistance, we calculate the effective resistance change in terms of the weighted graph Laplacian of the network.

To analytically predict the effect of a topological change, we start by adapting formulas for the effective resistance from Refs. [50, 53]. Recall that the weighted Laplacian \mathcal{L} is rank $N - 1$. We use a tilde in this section to indicate that one node has voltage set to zero (grounded), and its corresponding element is removed from all vectors and matrices. For example, if node j is grounded then

$$\tilde{\mathcal{L}}_{i,k} = \begin{cases} \mathcal{L}_{i,k} & \text{if } i, k < j, \\ \mathcal{L}_{i-1,k} & \text{if } i > j, k < j, \\ \mathcal{L}_{i,k-1} & \text{if } i < j, k > j, \\ \mathcal{L}_{i-1,k-1} & \text{if } i, k > j. \end{cases}$$

While the effective resistance does not depend on the choice of applied current I_0 , we include it in this derivation to keep units consistent. We write the current injection vector from Eq. (2) as $\tilde{\mathcal{I}} = I_0(\tilde{\mathbf{e}}_i - \tilde{\mathbf{e}}_j)$ where \mathbf{e}_i is the standard basis vector with 1 in element i and zero elsewhere. Then the effective resistance across node i and j is

$$R_{\text{eff}}^{ij} = \frac{(\tilde{\mathbf{e}}_i - \tilde{\mathbf{e}}_j)^\top \tilde{\mathcal{L}}^{-1} I_0 (\tilde{\mathbf{e}}_i - \tilde{\mathbf{e}}_j)}{I_0}.$$

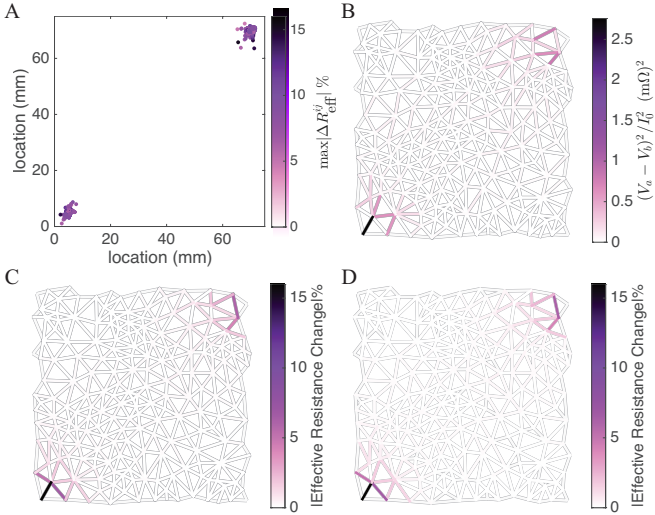


Figure 6. A: Scatter plot of the location and the magnitude of the maximum effective resistance change found in each network, under the edge flip enumeration test. These networks are the same as those used to generate Fig. 1B: 20 different initial point clouds at each Lloyd’s iteration $L = 0$ to $L = 100$. B: Heatmap of the voltage difference scaled by the applied current, $(V_a - V_b)^2/I_0^2$, for each edge in the network. C: Heatmap of Eq. (6) scaled by the initial effective resistance. D: Heatmap of the magnitude of the relative effective resistance change after flipping the diagonal edge within convex quadrilaterals in the network. Boundary edges and those not part of a convex quadrilateral are not flipped, and are colored white (i.e. zero).

Taking into account that node j is grounded ($\tilde{\mathbf{e}}_j$ is a vector of zeros) we have that

$$R_{\text{eff}}^{ij} = [\tilde{\mathcal{L}}^{-1}]_{ii}.$$

An edge flip first deletes an edge, then adds an edge. Deleting the edge connecting nodes a and b is a rank-1 update to the weighted graph Laplacian, given by

$$\tilde{\mathcal{L}}' = \tilde{\mathcal{L}} - \frac{1}{R_{ab}}(\tilde{\mathbf{e}}_a - \tilde{\mathbf{e}}_b)(\tilde{\mathbf{e}}_a - \tilde{\mathbf{e}}_b)^\top,$$

where R_{ab} is the true resistance of edge ab . Then, using the Sherman–Morrison formula [47], we rewrite the inverse of this rank-1 updated matrix as the inverse of the original matrix with a rank-1 update, given by

$$\tilde{\mathcal{L}}'^{-1} = [\tilde{\mathcal{L}}^{-1}]_{ii} + \frac{\frac{1}{R_{ab}} \left([\tilde{\mathcal{L}}^{-1}(\tilde{\mathbf{e}}_a - \tilde{\mathbf{e}}_b)]_i \right)^2}{1 - \frac{1}{R_{ab}}(\tilde{\mathbf{e}}_a - \tilde{\mathbf{e}}_b)^\top \tilde{\mathcal{L}}^{-1}(\tilde{\mathbf{e}}_a - \tilde{\mathbf{e}}_b)}.$$

Note that

$$(\tilde{\mathbf{e}}_a - \tilde{\mathbf{e}}_b)^\top \tilde{\mathcal{L}}^{-1}(\tilde{\mathbf{e}}_a - \tilde{\mathbf{e}}_b) \equiv R_{\text{eff}}^{ab}$$

and

$$[\tilde{\mathcal{L}}^{-1}(\tilde{\mathbf{e}}_a - \tilde{\mathbf{e}}_b)]_i \equiv \frac{V_a - V_b}{I_0}.$$

Thus, $\Delta R_{\text{eff}}^{ij} = [\tilde{\mathcal{L}}'^{-1}]_{ii} - [\tilde{\mathcal{L}}^{-1}]_{ii}$ is given by

$$\Delta R_{\text{eff}}^{ij} = \frac{(V_a - V_b)^2}{I_0^2} \frac{1}{R_{ab} - R_{\text{eff}}^{ab}}. \quad (5)$$

An edge flip is an edge deletion followed by an edge addition, so we can approximate the change in R_{eff} under an edge flip from edge ab to edge cd by

$$\Delta R_{\text{eff}}^{ij} \approx \frac{(V_a - V_b)^2}{I_0^2(R_{ab} - R_{\text{eff}}^{ab})} - \frac{(V_c - V_d)^2}{I_0^2(R_{cd} + R_{\text{eff}}^{cd})}. \quad (6)$$

From Eq. (6) we see that a simple physical quantity—the edge voltage difference—is a strong predictor of the magnitude of ΔR_{eff} . This explains why edges near the source and sink nodes have the largest affect, as they too have the largest voltage difference. In Fig. 6B we plot $(V_a - V_b)^2/I_0^2$, the square of the voltage difference across each edge scaled by I_0 . The second term in Eq. (6) accounts for the voltage difference across the edge to be added. Equation (6) fully accounts for the change in effective resistance, as shown in Fig. 6C; compare to Fig. 6D, the result of the edge flip test. Note that Eq. (6) would be exact if R_{eff}^{cd} were to be recomputed after the deletion of edge ab .

C. Local Tortuosity Change Correlates with Size of Effective Resistance Jumps

In two-phase heterogeneous materials, one can show that the effective resistivity of a material is related to the tortuosity of its conducting phase (see Eq. (13.226) in Ref. [56]). The tortuosity has been computed for disordered network-based two-phase heterogeneous materials [11]. To connect with the materials literature, we examine the relationship between the changes in network tortuosity (see Eq. (4)) and effective resistance in our networks. Having identified that network edge flips near

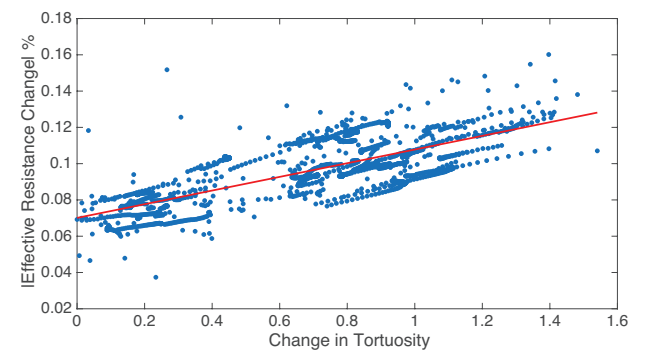


Figure 7. Scatter plot of change in quadrilateral tortuosity vs. its change in effective resistance when its diagonal edge is flipped. Quadrilaterals are taken from Fig. 6A. The solid red line is a least-squares fit line to the data with $R^2 = 0.5804$ and Pearson correlation coefficient of $r = 0.7619$, indicating a strong positive linear correlation.

either the source or sink nodes contribute the most to jumps in the effective resistance, we compute the tortuosity locally as opposed to over a larger portion of the network. In Fig. 7 we show the correlation between the change in tortuosity computed using Eq. (4) and the magnitude of change in effective resistance when an edge flip is performed on a quadrilateral structure in the network with one of its nodes being either the source or the sink node. The strong linear correlation ($r = 0.7619$ and $R^2 = 0.5804$) suggests that the local geometry and shortest paths in the vicinity of the source and sink nodes are both related to large changes in the network's effective resistance. Thus, the relationship between tortuosity and effective resistance observed for materials is also relevant to spatially embedded resistor networks.

D. Finite-Size Effects

We have shown the sensitivity of R_{eff} measured diagonally across a network to single topological changes in the network near the source and sink nodes. In this section, we show that the resistance of a network is less sensitive to individual topological changes if more of the network topology is averaged over by a single measurement. Specifically, we show that summing R_{eff} calculated between every pair of nodes in the network, the total effective resistance in Eq. (3), is less sensitive to single topological changes. Similarly, increasing the network size decreases the sensitivity of R_{eff} to single topological changes.

In Fig. 8A, we plot the total effective resistance, Eq. (3), as a function of Lloyd's iteration number L with each curve representing a different initial point cloud. Comparing to Fig. 1, we see overall a small spread of values and a noticeable lack of large jumps between sequential Lloyd's iterations. The results of conducting the edge-flip test on both the square lattice with diagonals and a sample random network (generated with the method described in Sec. II A) are shown in Figs. 8B and C, respectively. Note the decrease in percentage change from around 10% maximum for R_{eff} down to 0.35% for R_{tot} .

While the overall importance of a single edge is reduced in the case of R_{tot} relative to R_{eff} , we still observe how local topological changes affect this global measure of the network's electrical transport. Figure 8B shows the result of the edge flip test for the square lattice with diagonals across each cell (same network as Fig. 4A). Despite R_{tot} being a global quantification of the network, unlike R_{eff} that has an added directionality due to the diagonal chosen to measure across, we see a directionality in the response of R_{tot} to the edge flip test. Diagonal edges near the northwest and southeast corners have a larger effect than other diagonal edges. Additionally, we see that edges parallel to the boundary have a large effect, with this effect being largest for the middle of the outermost ring of interior edges. This effect is also ap-

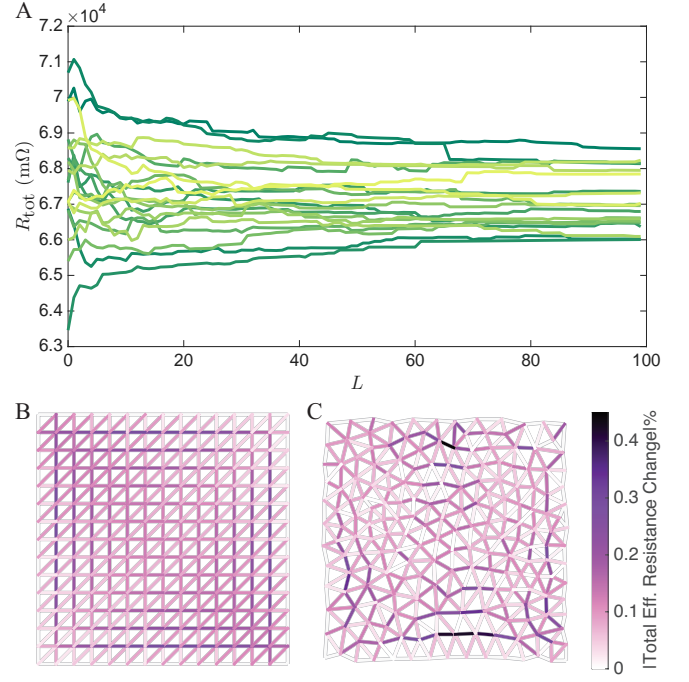


Figure 8. A: Total effective resistance, R_{tot} computed from Eq. (3), as a function of Lloyd's iteration number L . Each curve is the evolution of a different initial point cloud. B: Heatmap where the color of each edge indicates the magnitude of the relative percent change of the total resistance, R_{tot} , when the edge is flipped to the other diagonal of its quadrilateral. Same network as Fig. 4A. C: Same as B but for a disordered network at $L = 10$. In both B and C, boundary edges and those not part of a convex quadrilateral are not flipped, and are colored white (i.e. zero).

parent in the disordered network in Fig. 8C with edges not only near, but parallel to the boundary, having the greatest effect. It appears that edge flips that help create pathways into the interior of the network near the boundary affect the total effective resistance the most.

Another way to decrease the importance of a single edge is to increase the total number of edges by creating larger networks with more points inside the same-sized box. This decreases the overall size of each edge and also increases the number of pathways between any two nodes, thus intuitively changing any one edge should have a smaller effect. This is confirmed in Fig. 9, which plots the result of performing the edge-flip test and recording the maximum magnitude of percent change in R_{eff} for each of 20 networks at each Lloyd's iteration number. (For $N = 200$ an additional 80 networks were averaged over to decrease statistical error.) The solid curve is the average over this ensemble, and the shaded region is one standard error above and below. As the number of nodes N increases, the maximum percentage change decreases, further supporting jumps in R_{eff} (and R_{tot}) are finite-size effects. These finite size effects are important to understand from a practical standpoint because of the size limitations imposed by the processes used to create

network metamaterials, which typically involve additive manufacturing (see, e.g., [4, 19, 20]).

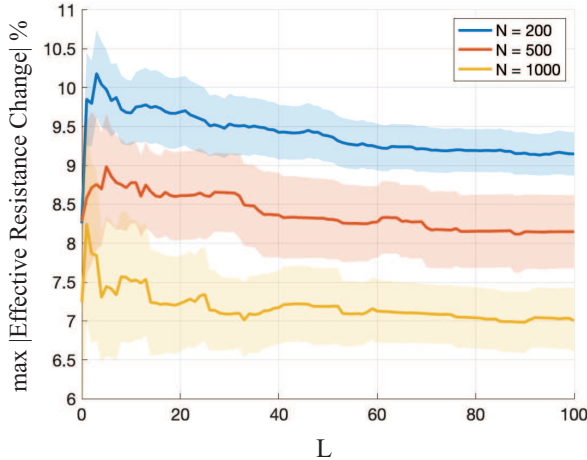


Figure 9. The solid curves depict the mean of the maximum effective resistance change across the ensemble of 100 networks for $N = 200$ and 20 networks each for $N = 500$ and $N = 1000$ under flip test with standard errors added as colored regions.

E. Voronoi Tessellation

As described in Fig. 3, the local topological changes associated with Delaunay networks result in abrupt changes in effective resistance under point cloud perturbation. While the effect of local topological changes on the effective and total resistance of the network is universal, we only observe such large jumps between Lloyd’s algorithm iterations when constructing networks with the Delaunay triangulation. To illustrate this, we discuss R_{eff} of a Voronoi tessellation on the underlying point cloud.

With the same 20 simulations of a point cloud evolved under 100 iterations of Lloyd’s algorithm used in Fig. 1, we form the networks using a Voronoi tessellation constructed inside the bounded square domain. Figure 10 shows R_{eff} measured across the northeast-southwest diagonal of the aforementioned networks. In stark contrast to the Delaunay networks shown in Fig. 1B, the Voronoi networks’ effective resistances in Fig. 10 evolve more smoothly as Lloyd’s algorithm is iteratively applied. Small perturbations to the point cloud in turn cause small perturbations to the length of edges in the Voronoi polygons, with topological changes (addition or removal of edges) occurring as a limit of vanishing edge length. By contrast, the topological changes in the Delaunay triangulation tend to involve longer edges, which tends to result in more drastic changes in R_{eff} .

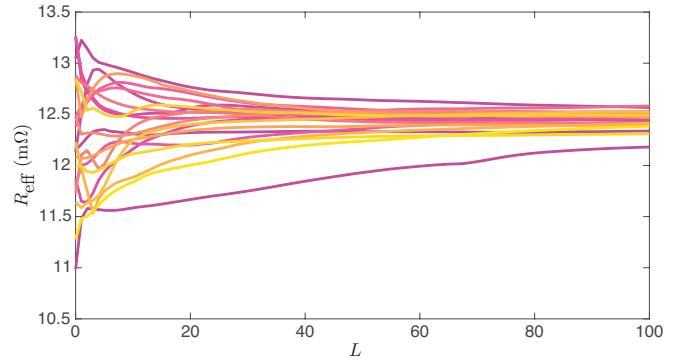


Figure 10. Ensembles of effective resistance across northeast-southwest diagonal for Voronoi tessellated networks. These Voronoi networks are generated with the same point clouds that generated the previous Delaunay networks.

IV. DISCUSSION AND CONCLUSIONS

In this paper, we showed how the location and directionality of a topological change in a network influences the change in the network’s effective and total resistances, R_{eff} and R_{tot} , respectively. Seeking to understand sharp changes in R_{eff} observed in Ref. [4] as the point cloud underlying the Delaunay triangulation-based network evolved smoothly under Lloyd’s algorithm, we focused on Delaunay triangulation networks and the Delaunay flip topological change. The Delaunay flip is an abrupt swapping of which diagonal in a convex quadrilateral structure in the network is connected by an edge. For the effective resistance measured diagonally across the network as in Ref. [4], the addition of edges or Delaunay flips near the source and sink nodes had the largest effect. For R_{tot} , edges near and parallel to the boundary when flipped had the largest effect.

We further explained the locational-dependence of Delaunay flips on R_{eff} by analytically approximating the flip as two independent rank-one changes to the weighted combinatorial graph Laplacian and computing its inverse using the Sherman–Morrison formula [47]. This revealed the change in effective resistance is proportional to the voltage difference across the nodes of the added and removed edges, which in turn is largest for edges near the source and sink nodes. Moreover, to relate our mathematical network model to the heterogeneous network materials it emulates, we computed the change in tortuosity across quadrilaterals containing the source and sink nodes and compared that to the change in effective resistance. We found a strong positive correlation between the change in tortuosity and effective resistance, which is consistent with the expectation from the materials literature [56].

Large changes in either R_{eff} or R_{tot} correlate to how efficiently current can be transported away from boundaries. In the case of R_{eff} , we specifically measured between two nodes on the boundary (opposite corners of a network) finding edges that disrupt or enhance the

pathway across the network have the largest effect, especially when no other edges in the local neighborhood can support the disruption. For R_{tot} , we found that edges originally parallel to the network boundary produce the largest changes to the resistance when flipped. Such a large change in resistance occurs because these flipped edges now offer a more direct pathway for electrical transport away from the network boundary. Overall, we see some relationship to shortest paths in the network, but a shortest path alone cannot completely describe either the effective resistances nor predict the effect of single topological changes. Similarly, other network statistics like edge betweenness that are able to predict failure processes in materials [43] fail to predict the magnitude of the changes in R_{eff} [4]. While we focused here on how topological changes in particular regions of the network effect R_{eff} , the quantification of the relationship between transport and global network characteristics as a function of disorder and tessellation type is also of interest (see, e.g., Ref. [57]).

The effect of individual topological changes is a finite-size effect. The total effective resistance is the summation of all the pairwise effective resistances; it averages over more of a network and each individual edge is less important. Thus, we saw an order of magnitude decrease in the percentage change of R_{tot} over R_{eff} . Furthermore, we saw a decrease in the maximum percent change of R_{eff} as the network size is increased. From a material design point of view, the effect of local topological changes remains an important effect to study due to the practical limitations in network size imposed by the additive manufacturing methods commonly used to make network metamaterials (e.g., in Refs. [4, 19, 20]). Understanding which local regions of the network produce the largest change can guide optimization routines in this high-dimensional design space to manufacture disordered network metamaterials with tailored transport properties.

Additionally, the appearance of abrupt jumps in R_{eff}

and R_{tot} under the evolution of the underlying point cloud using Lloyd's algorithm is a product of applying the Delaunay triangulation to the point cloud. We showed that using a Voronoi tessellation instead removes these abrupt changes, which is advantageous for using optimization algorithms to tailor the electric transport properties of a network. Typical gradient-based optimization algorithms acting on the node positions will encounter issues due to the large jumps in R_{eff} that accompany the Delaunay triangulation topological changes, while the Voronoi tessellation, whose R_{eff} varies more smoothly as its progenitor points are perturbed, will be less problematic. If instead an optimization is desired over a network configuration with fixed nodes and movable edges, the prediction of replacing one edge with another and its proportionality to voltage differences across the old and new edge remains applicable regardless of whether or not the edges are the two diagonals of a convex quadrilateral.

ACKNOWLEDGMENTS

The authors would like to thank Karen E. Daniels for insightful discussions and Mason A. Porter for helpful feedback on the manuscript. This work is supported by the collaborative NSF DMREF Grant No. CMMI-2323342 and NSF Grant No. DMS-2307297.

DATA AVAILABILITY

The code to generate and evolve a point cloud using Lloyd's algorithm is available on GitHub [58]. The code to compute the effective resistance, total effective resistance, and execute the edge flip enumeration test is available on GitHub [59]. The set of 20 $N = 200$ node networks is generated from the same evolving point clouds used in Ref. [4] and are available on Dryad [60].

[1] C. Broedersz and F. MacKintosh, Modeling semiflexible polymer networks, *Reviews of Modern Physics* **86**, 995 (2014).

[2] P. S. Stewart and S. H. Davis, Dynamics and stability of metallic foams: Network modeling, *Journal of Rheology* **56**, 543–574 (2012).

[3] A. A. Moreira, C. L. N. Oliveira, A. Hansen, N. A. M. Araújo, H. J. Herrmann, and J. S. Andrade, Fracturing highly disordered materials, *Physical Review Letters* **109**, 255701 (2012).

[4] C. Obrero, M. Tirfe, C. Lee, S. Saptarshi, C. Rock, K. E. Daniels, and K. A. Newhall, Electrical transport in tunably disordered metamaterials, *Physical Review E* **112**, 035505 (2025).

[5] H. Wang, M. A. G. Cunha, J. C. Crocker, and A. J. Liu, Mechanosensitive remodeling sustains rigidity homeostasis in actin cortex models (2025), iSSN: 2692-8205 Pages: 2025.10.05.680567 Section: New Results.

[6] F. Barrows, G. Zhang, S. Anand, Z. Chen, J. Lin, A. Desai, S. Martiniani, and F. Caravelli, A unifying approach to self-organizing systems interacting via conservation laws (2025), arXiv:2507.02575 [cond-mat].

[7] P. H. Nardelli, N. Rubido, C. Wang, M. S. Baptista, C. Pomalaza-Raez, P. Cardieri, and M. Latva-aho, Models for the modern power grid, *The European Physical Journal Special Topics* **223**, 2423–2437 (2014).

[8] M. Barthelemy, *Spatial Networks: A Complete Introduction: From Graph Theory and Statistical Physics to Real-World Applications* (Springer International Publishing, Cham, Switzerland, 2022).

[9] S. Fulco, M. K. Budzik, H. Xiao, D. J. Durian, and K. T. Turner, Disorder enhances the fracture toughness of 2D mechanical metamaterials, *PNAS Nexus* **4**, pgaf023 (2025).

[10] Y. Jiao, Exotic acoustic-edge and thermal scaling in disordered hyperuniform networks (2025), arXiv:2510.25136

[cond-mat].

[11] S. Torquato and D. Chen, Multifunctional hyperuniform cellular networks: optimality, anisotropy and disorder, *Multifunctional Materials* **1**, 015001 (2018).

[12] A. Montiel, T. Nguyen, C. L. Rountree, V. Geertsen, P. Guenoun, and D. Bonamy, Effect of architecture disorder on the elastic response of two-dimensional lattice materials, *Physical Review E* **106**, 015004 (2022).

[13] M. Skolnick and S. Torquato, Effective transport and mechanical properties of two-phase materials across the order-disorder spectrum, *Acta Materialia* **290**, 120921 (2025).

[14] A. T. Chieco and D. J. Durian, Quantifying the long-range structure of foams and other cellular patterns with hyperuniformity disorder length spectroscopy, *Physical Review E* **103**, 062609 (2021).

[15] E. Newby, W. Shi, Y. Jiao, S. Torquato, and R. Albert, From point patterns to networks: to what extent does the Delaunay triangulation reproduce key spatial and density information? *Journal of Complex Networks* **13**, cnaf040 (2025).

[16] C. E. Maher and K. A. Newhall, Characterizing the hyperuniformity of disordered network metamaterials, *Physical Review E* **111**, 065420 (2025).

[17] L. Siedentop, G. Lui, G. Maret, P. M. Chaikin, P. J. Steinhardt, S. Torquato, P. Keim, and M. Florescu, Stealthy and hyperuniform isotropic photonic band gap structure in 3D, *PNAS Nexus* **3**, pgae383 (2024).

[18] D. R. Reid, N. Pashine, J. M. Wozniak, H. M. Jaeger, A. J. Liu, S. R. Nagel, and J. J. de Pablo, Auxetic metamaterials from disordered networks, *Proceedings of the National Academy of Sciences* **115**, E1384 (2018).

[19] M. Shen, M. A. Reyes-Martinez, L. A. Powell, M. A. Iadicola, A. Sharma, F. Bylén, N. Pashine, E. P. Chan, C. L. Soles, H. M. Jaeger, and J. J. de Pablo, An autonomous design algorithm to experimentally realize three-dimensionally isotropic auxetic network structures without compromising density, *npj Computational Materials* **10**, 113 (2024).

[20] K. Moody, M. Li, C. E. Maher, K. Lee, T. Horn, K. A. Newhall, R. Hurley, K. E. Daniels, and C. Rock, A methodology for manufacturing 3D disordered metamaterials using laser powder bed fusion from granular packings and hyperuniform point clouds, *Additive Manufacturing* (2026), (*under review*).

[21] D. Chen, Y. Zheng, L. Liu, G. Zhang, M. Chen, Y. Jiao, and H. Zhuang, Stone–Wales defects preserve hyperuniformity in amorphous two-dimensional networks, *Proceedings of the National Academy of Sciences* **118**, 10.1073/pnas.2016862118 (2021).

[22] P. Alonso Ruiz, Power dissipation in fractal Feynman–Sierpinski AC circuits, *Journal of Mathematical Physics* **58**, 073503 (2017).

[23] J. P. Chen, L. G. Rogers, L. Anderson, U. Andrews, A. Brzoska, A. Coffey, H. Davis, L. Fisher, M. Hansalik, S. Loew, and A. Teplyav, Power dissipation in fractal AC circuits, *Journal of Physics A: Mathematical and Theoretical* **50**, 325205 (2017).

[24] A. Muranova, Effective impedance over ordered fields, *Journal of Mathematical Physics* **62**, 033502 (2021).

[25] A. Muranova, On the effective impedance of finite and infinite networks, *Potential Analysis* **56**, 697 (2022).

[26] A. Muranova, On the notion of effective impedance, *Operators and Matrices* **14**, 723 (2020).

[27] A. Muranova and R. Schippa, Eigenvalues of the normalized complex Laplacian on finite electrical networks (2020), arXiv:2012.12759 [math].

[28] A. Muranova and W. Woess, Networks with complex weights: Green function and power series, *Mathematics* **10**, 820 (2022).

[29] C. R. Paul, *Analysis of Multiconductor Transmission Lines* 2nd ed. (Wiley-IEEE Press, Hoboken, NJ, 2018).

[30] S. H. Strub and L. Böttcher, Modeling deformed transmission lines for continuous strain sensing applications, *Measurement Science and Technology* **31**, 035109 (2019).

[31] L. Böttcher and M. A. Porter, Dynamical processes on metric networks, *SIAM Journal on Applied Dynamical Systems* **24**, 2848–2885 (2025).

[32] M. Bartkowiak and G. D. Mahan, Nonlinear currents in Voronoi networks, *Physical Review B* **51**, 10825 (1995).

[33] R. G. Morris and M. Barthelemy, Transport on coupled spatial networks, *Physical Review Letters* **109**, 128703 (2012).

[34] B. He, A. Ye, S. Chi, P. Mi, Y. Ran, L. Zhang, X. Zou, B. Pu, Q. Zhao, Z. Zou, D. Wang, W. Zhang, J. Zhao, M. Avdeev, and S. Shi, CAVD, towards better characterization of void space for ionic transport analysis, *Scientific Data* **7**, 153 (2020).

[35] N. Masuda, M. A. Porter, and R. Lambiotte, Random walks and diffusion on networks, *Physics Reports* **716–717**, 1 (2017).

[36] P. G. Doyle and J. L. Snell, *Random walks and electric networks*, Carus Mathematical Monographs No. v. 22 (Mathematical Association of America, Washington, D.C., 1984).

[37] I. García-Redondo, C. Landi, S. Percival, A. Skeja, B. Wang, and L. Zhou, Effective resistance in simplicial complexes as bilinear forms: generalizations and properties (2025), arXiv:2511.10749 [math].

[38] M. J. Gu, S. Lin, X. F. Xu, C. R. Wang, B. H. Wu, and J. C. Cao, Random-resistor network modeling of resistance hysteresis of vanadium dioxide thin films, *Journal of Applied Physics* **132**, 015301 (2022).

[39] S. Lloyd, Least squares quantization in PCM, *IEEE Transactions on Information Theory* **28**, 129 (1982).

[40] L. Papadopoulos, M. A. Porter, K. E. Daniels, and D. S. Bassett, Network analysis of particles and grains, *Journal of Complex Networks* **6**, 485 (2018).

[41] L. A. Torres-Sánchez, G. T. Freitas De Abreu, and S. Kettemann, Analysis of the dynamics and topology dependencies of small perturbations in electric transmission grids, *Physical Review E* **101**, 012313 (2020).

[42] S. Gnutzmann, Topological resonances in scattering on networks (graphs), *Physical Review Letters* **110**, (2013).

[43] E. Berthier, M. A. Porter, and K. E. Daniels, Forecasting failure locations in 2-dimensional disordered lattices, *Proceedings of the National Academy of Sciences* **116**, 16742 (2019).

[44] A. Sanner, L. Michel, A. Lingua, and D. S. Kammer, Less is more: removing a single bond increases the toughness of elastic networks *International Journal of Fracture* **249**, 78 (2025).

[45] E. Young and M. A. Porter, Dynamical importance and network perturbations, *Physical Review E* **110**, 064304 (2024).

[46] V. Tejedor, O. Bénichou, R. Voituriez, and M. Moreau, Response to targeted perturbations for random walks on networks, *Physical Review E* **82**, 056106 (2010).

